Scientific Research Publishing

Open Journal of Applied Sciences, 2024, 14, 2559-2579
https://www.scirp.org/journal/ojapps
ISSN Online: 2165-3925
ISSN Print: 2165-3917

Innovative Methods of Synthesis and Characterization for Molecularly Imprinted Polymers

Youyao Luo

School of Chemistry and Materials Science, Langfang Normal University, Langfang, China
Email: lfsfxyxinxigongkai@126.com

How to cite this paper: Luo, Y.Y. (2024) Innovative Methods of Synthesis and Characterization for Molecularly Imprinted Polymers. *Open Journal of Applied Sciences*, **14**, 2559-2579.
https://doi.org/10.4236/ojapps.2024.149169

Received: August 15, 2024
Accepted: September 23, 2024
Published: September 26, 2024

Abstract

The characterization of these molecularly imprinted polymers is essential to understanding their binding dynamics and structural properties. Through the analysis of the current research, it is found that there are overlaps in the methods used by scholars. The Langmuir equation is frequently applied to model the adsorption isotherms of MIPs, providing critical insight into the capacity and affinity of the binding sites. Infrared Spectroscopy (IR) plays a crucial role in identifying the functional groups involved in the imprinting process and confirming the successful formation of specific binding sites. UV-visible spectrophotometry is employed to monitor the absorption characteristics of the polymers, offering data on the interactions between the template molecules and the polymer matrix. Transmission Electron Microscopy (TEM) provides detailed visualization of the internal structure of MIPs at the nanoscale, revealing the morphology and size of the imprinted cavities. Thermogravimetric Analysis (TGA) assesses the thermal stability and composition of the polymers, identifying decomposition patterns that are indicative of the material's robustness under different conditions. Finally, the Laser Particle Size Analyzer is used to measure the size distribution of the polymer particles, which is critical for determining the uniformity and efficiency of the imprinting process. The six characterization methods discussed in this paper provide a comprehensive understanding of MIP, and it is hoped that in the future, more optimized design solutions will emerge and their applications in various fields will be enhanced.

Keywords

Molecularly Imprinted Polymers, Langmuir Equation, Infrared Spectroscopy, UV Visible Spectrophotometry, Transmission Electron Microscopy

1. Background

1.1. What Is MIP

Molecular imprinting technology is an efficient separation and molecular recognition technique used to synthesize molecular polymers with specific molecular recognition capabilities [1]. MIP is easy to prepare with good chemical stability, low cost, strong affinity and specificity, and is used to improve the recognition selectivity and detection sensitivity of target molecules. After removing the template from the polymer, specific imprinting cavities are left which can be recombined with the target molecule based on size, shape, and functional binding sites. It has selectivity for a specific type or class of analytes and can be used for the extraction and determination of target substances in complex samples [2]. It is used to react with the target substance, improving accuracy and efficiency.

1.2. Application of MIP

MIP is applied in various fields, such as healthcare, environmental testing, food safety, etc. The use of MIP technology in surface water can selectively identify and remove target antibiotics from environmental pollutants [3]; it is also possible to separate and enrich carbamate pesticides in the environment [4], thereby reducing the risks of ecological environment to human health. The use of MIP technology in drugs can selectively identify target substances with similar structures and related chemical substances in complex samples, and can be applied to the safety analysis and environmental monitoring of veterinary drug residues in feed and animal food, improving the efficiency of drug detection [5].

2. Theory

At present, there are various synthesis methods for molecularly imprinted polymers, such as microfluidic technology, chemical grafting method, sacrificial carrier method, and controllable free radical polymerization method. Through various studies, the technology has been optimized in traditional methods, not only from the perspective of time speed but also from the perspective of synthesis speed which has been improved.

2.1. Microfluidic Technology

As an advanced technology, it has been widely used in the synthesis of polymers in recent years. Compared with traditional synthesis methods, it has significant advantages, such as low reagent consumption, strong controllability, short preparation time, continuous production, and efficient heat and mass transfer characteristics. Currently, some experiments have introduced imprinting polymerization reactions into micro reaction channels, achieving microfluidic synthesis of molecularly imprinted polymers.

Combining molecular imprinting with microfluidic technology to synthesize

shikimic acid imprinted polymers through microfluidic methods. The advantages of microfluidics include fast, continuous, high efficiency, high mass and heat transfer performance. The shikimic acid imprinted polymer was synthesized in a microchannel through the sol gel method using Tetraethoxysilane (TEOS) as the crosslinking agent, APTES as the functional monomer, shikimic acid as the template, and ammonia as the catalyst. This method has the advantages of short synthesis time, continuous synthesis, high productivity, etc. [6].

2.2. Chemical Grafting Method

Chemical grafting is a rapidly developing and widely used polymerization method since the development of surface molecular imprinting technology [7]. It mainly covers the surface of the substrate with imprinted polymers through chemical bonding or self-assembly, forming surface molecular imprinted polymers and obtaining core-shell structured nanoparticles. In recent years, chromatography media based on organic polymers have received increasing attention. Polymer based chromatography media compensate for the shortcomings of conventional agarose chromatography media in terms of mechanical strength and pore size. However, due to their large pore size and low specific surface area, protein binding capacity is low, especially for macroporous polymer chromatography media. To improve the adsorption capacity of the medium, grafting polymer ligands onto the surface of microspheres is a common strategy. By utilizing the characteristics of such molecules such as a large number of functional groups and variable molecular conformations, the capture efficiency of protein molecules can be improved.

Preparing an anion exchange chromatography medium using branched polyethyleneimine (PEI) as a ligand, increasing the number of amino groups on the surface of macroporous polyacrylate microspheres. At the same time, using the "chain transfer" mechanism of PEI long-chain molecules, they further improved the mass transfer of protein macromolecules inside the medium, thereby increasing the binding capacity and mass transfer rate of proteins [8].

2.3. Sacrificial Carrier Method

After using the sacrificial carrier method to prepare MIP and obtaining core-shell structured nanoparticles through chemical grafting, the core structure in the core-shell structure is removed through chemical or physical methods. The resulting hollow shell structure MIP has a higher specific surface area and larger adsorption capacity. However, in the process of removing the substrate, it is easy to damage the three-dimensional network structure of the polymer, so choosing an appropriate method to remove the substrate is crucial.

Using through flow silica gel as a carrier and sacrificial carrier method to prepare monodisperse through flow poly (MAA co EDMA) polymer stationary phase, which was used for protein chromatography separation under different modes.

The main advantages of this stationary phase are as follows: 1) It contains a penetrating skeleton structure, permeable macropores, and abundant mesopores, with a large specific surface area and high porosity, suitable for the separation of macromolecular proteins; 2) It has good biocompatibility and can effectively avoid non-specific protein adsorption; 3) It contains hydrophobic frameworks and abundant carboxyl groups, different chromatographic separation modes such as RPC/HIC/IEC can be converted by adjusting the composition of the mobile phase; 4) It has characteristics such as low back pressure and high mass transfer, and can achieve rapid separation of macromolecular proteins [9].

2.4. Active Controllable Free Radical Polymerization Method

Active controllable free radical polymerization is a polymerization method developed on the basis of chemical grafting, which provides effective methods for achieving controllable polymerization. It is mainly divided into atom transfer free radical polymerization (ATRP), reversible addition broken chain transfer polymerization (RAFT), and other mediated free radical polymerization methods. The reaction conditions for preparing molecularly imprinted polymers using ATRP method are mild, which can effectively control the thickness of the polymer layer, and the prepared material has good dispersibility and is not prone to agglomeration.

The traditional preparation method of molecular imprinting is due to the uncontrollability of free radical polymerization, which is manifested as slow initiation, fast growth, and rapid termination of the polymerization reaction. This can lead to a wide relative molecular weight distribution of the generated polymerization products, uncontrollable relative molecular weight and structure, and cause a certain degree of mismatch, resulting in a decrease in the selectivity of the polymer. However, the use of reversible addition fragmentation chain transfer radical (RAFT) reagents can achieve efficient polymerization of various monomers. The use of this reagent in polymerization reactions can make the polymerization reaction mild and controllable. The resulting molecularly imprinted polymers have characteristics such as controllable relative molecular weight and narrow relative molecular weight distribution, which can adsorb more target molecules and improve selectivity. Therefore, the use of RAFT reagents can effectively improve the morphology and adsorption capacity of the polymers. At present, RAFT reagents have been used in the preparation of molecularly imprinted polymers for regulation.

Preparing molecularly imprinted polymers of resveratrol with special affinity using RAFT reagents and applied them to the separation and analysis of resveratrol in grape skins, achieving good separation efficiency [10].

3. Characterization Methods

3.1. Langmuir Equation

Langmuir's research suggests that atoms or molecules on solid surfaces have

residual valence forces outward, which can capture gas molecules. The range of action of this residual valence force is equivalent to the molecular diameter, so only single-layer adsorption can occur on the surface of the adsorbent.

Table 1 shows the amount of lutetium (III.) ion-blotted polymer [Lu (III.)-MIP] adsorbed to lutetium ions and the initial concentration of lutetium (III.) ions in solution. The relationship curve between C/Q and C based on experimental data shows an approximately linear relationship, indicating that the adsorption of Lu^{3+} by Lu MIP conforms to the Langmuir adsorption isotherm equation: $C_{eq}/Q_{eq} = C_{eq}/Q_{\max} + 1/(Q_{\max} \times K)$, where C_{eq} is the equilibrium adsorption capacity, $Q_{\max}$ is the saturation adsorption capacity, and K is a constant. Further exploration of the adsorption capacity of lutetium (III) ion imprinted polymer [Lu (III) - MIP] on lutetium (III) ions as a function of the initial concentration of lutetium (III) ions in the solution [11].

Table 1. Concentration and adsorption capacity.

$C/(mg \cdot L^{-1})$	A_1	A_2	$Q/(mg \cdot L^{-1})$	$C/Q(g \cdot L^{-1})$
20	0.356	0.105	2.8	7.14
40	0.405	0.135	5.3	7.55
160	0.845	0.42	16.1	9.94
320	0.722	0.328	34.93	9.09
640	1.528	1.024	45.15	14.29
1280	3.201	2.521	54.38	23.55
1750	1.975	1.645	58.48	29.92
2500	2.028	1.842	63.58	39.32
3500	2.498	2.320	64.20	54.52
4500	2.498	2.322	63.41	70.97

Based on the experimental data, a linear graph is generated for the Lu-MIP adsorption isotherm (Figure 1), the equation is derived by calculating the relevant coefficients. The maximum adsorption capacity can be obtained based on the equation, and then compared with the saturated adsorption capacity. It shows that as the concentration of lutetium (III) ions increases, the adsorption capacity first gradually increases, and finally tends to plateau, reaching saturation.

The fitting parameters can be calculated by experimenting with MIP and NIP on Ph, 2-MP, 3-MP and 2-CP (Table 2) and fitting the adsorption isotherms of LI and L-FI. Both models fit the experimental data well, with very good R2 and RSS values and low relative errors. The adsorption capacity was compared with the two models. [12]

By comparing Figure 2 and Figure 3, the applicability of the L-FI model to the

concentration range studied passed the suitability test, in which the binding affinity of the fitted analyzed K_0 was limited to $K_{max}(1/C_{min})$ and $K_{min}(1/C_{max})$. The relatively simple LI model can be applied more effectively when m in the L-FI model is close to 1, but the role of the L-FI model cannot be ignored because it can simulate subtle differences and thus better fit the experimental data. It was concluded that some of the higher MIP adsorption capacities could be attributed to the difference in the surface area of MIP and NIP. In addition, the three parameters (N_t a, and m) can give us more perspectives to understand the differences in adsorption behavior.

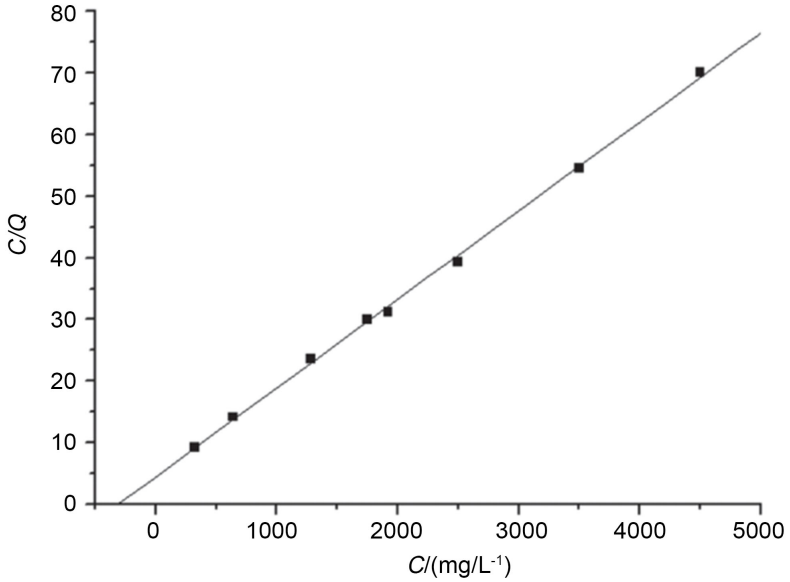

Figure 1. Lu-MIP adsorption isotherm.

Table 2. Comparison between the Binding Sites and Affinity Constants in LI, L-FI, and BET Models.

model	parameter	Ph	2-MP	3-MP	2-CP	4-OP
LI	N (μmol/g)	136	65.8	71.3	178	1445
	K (μM^{-1})	0.0043	0.0135	0.0119	0.0131	0.0038
L-FI	N_t (μmol/g)	124	98.9	93.0	225	313
	K limits (μM^{-1})	0.0048 - 0.099	0.0056 - 0.119	0.0056 - 0.118	0.0072 - 0.164	0.0124 - 0.282
BET	q_m n (μmol/g)[a]	89.3	73.3	71.6	186	137
	K_{ca} (composite affinity)[b]	0.0101	0.0128	0.0134	0.0132	0.0824
Statistics	average of modeled binding sites (μmol/g)	117	79.3	78.6	196	632
	RSD% for binding sites	21	22	16	13	112
	discrepancy% (between the LI and BET affinities	57	5.5	11	1.0	95

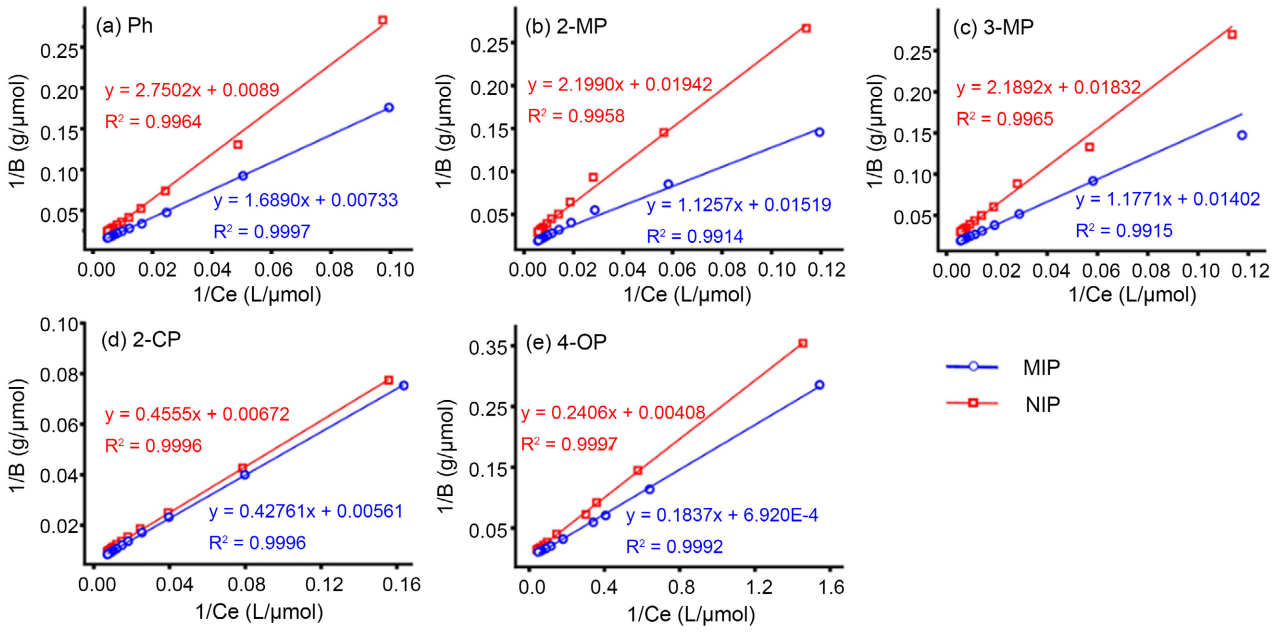

Figure 2. Experimental data for the individual study (circle points for MIP, squares points for NIP) were fit to an LI isotherm (solid lines) for MIP and NIP. (a) Ph. (b) 2-MP. (c) 3-MP. (d) 2-CP. (e) 4-OP.

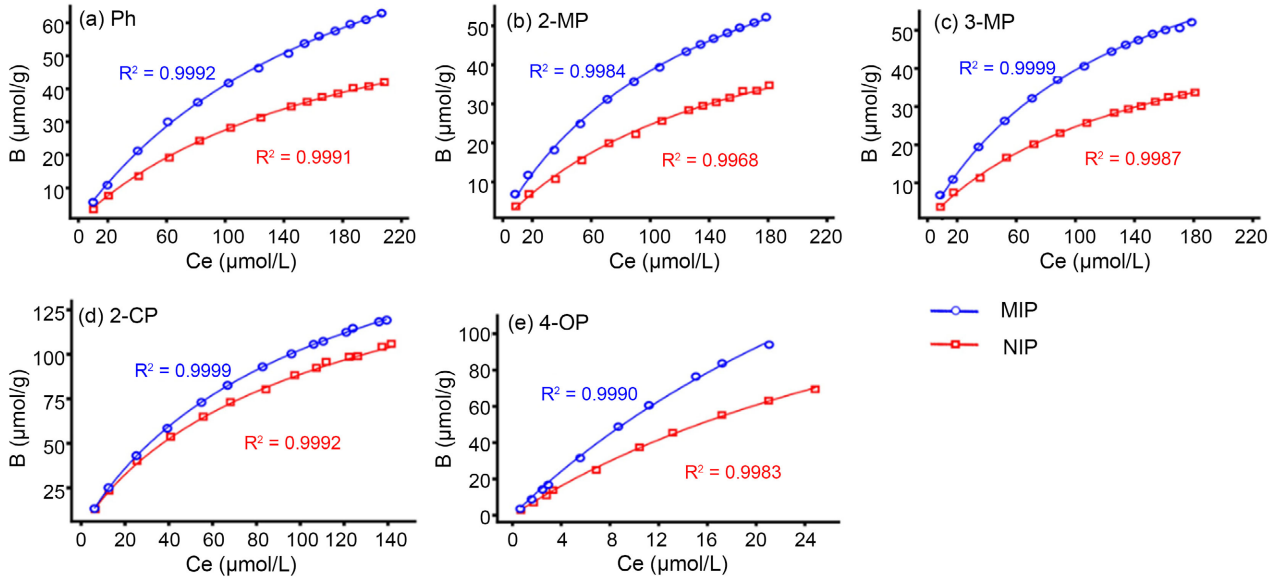

Figure 3. Experimental data for the individual study (circle points for MIP, squares points for NIP) were fit to an L-FI isotherm (solid lines) for MIP and NIP. (a) Ph. (b) 2-MP. (c) 3-MP. (d) 2-CP. (e) 4-OP.

3.2. Infrared Spectroscopy

The principle of an infrared spectrometer is that when a certain frequency of infrared light is focused on the analyzed sample, if the vibration frequency of a certain functional group in the molecule is the same as the frequency of the infrared radiation, resonance will occur, thereby absorbing a certain frequency of infrared radiation. By recording the absorption of infrared radiation by the molecule with the instrument, a comprehensive spectrum reflecting the characteristics of the

sample composition can be obtained, and the type and structure of the compound can be inferred.

The structure characterization and synthesis process stability of toluene molecularly imprinted polymers were investigated using the Magna750 Fourier transform infrared spectrometer [13]. By analyzing the peak beams displayed in the characteristic peaks of the infrared spectrum, functional groups may exist in the polymer, and the structure of the polymer can be inferred.

The upper part shows the results of 200 mg KBr mixed with 20 mg of toluene molecularly imprinted polymer; the lower part is the detection results of the toluene molecularly imprinted polymer.

By analyzing the beam of the infrared spectrum (**Figure 4**), it was found that the C-H stretching vibration occurred at 2928 cm^{-1}; The C=O stretching vibration peak in carboxylic acid is located at 1695 cm^{-1}; 1382 cm^{-1} is CH_3 symmetric bending vibration; At 1602 cm^{-1}, there is a symmetric stretching vibration peak of the benzene ring; At 510 cm^{-1}, there are different forms of ring stretching vibration peaks; 450 cm^{-1} is the lateral ring stretching vibration peak; The multiple peaks at 900 - 650 cm^{-1} are believed to be the successful reaction of the isomer of divinylbenzene (DVB) into the polymer. The absence of a peak at 749 cm^{-1} indicates that there is no monosubstituted benzene, indicating that the toluene molecule has been completely cleared. Further analysis of the infrared spectra of the two synthesized products revealed that the characteristic peaks of their infrared spectra basically overlapped, with no significant peak differences or impurities, indicating that the process was relatively stable.

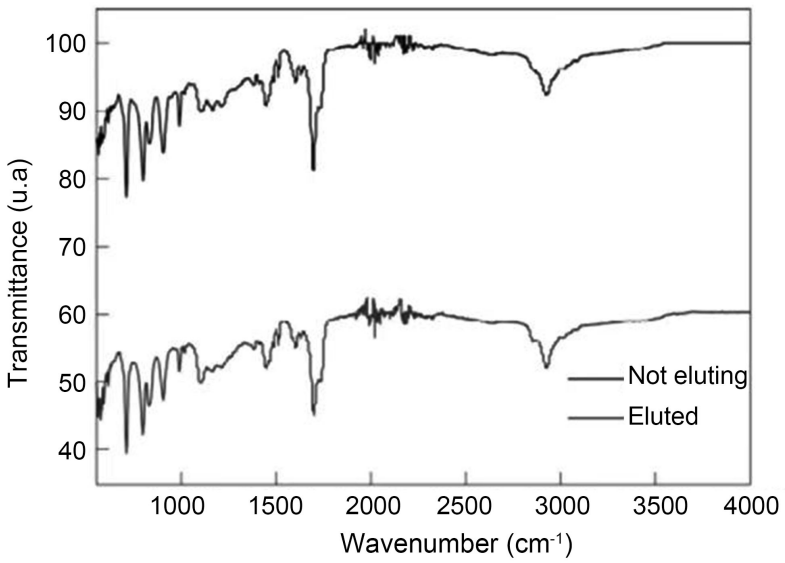

Figure 4. Infrared spectra of spherical toluene imprinted polymers.

By analyzing the functional groups using the characteristic beam obtained by the infrared spectrometer, further conclusions can be drawn about the removal of template molecules [14].

Methacrylic acid (MAA) was used as FM and chloroform as solvent to synthesize the most suitable MIP according to a 1:4 stoichiometry.

Figure 5 shows the presence of some characteristic bands, and the analysis of wavenumbers shows that 2892 cm^{-1} is the C-H stretch of sp^3 carbon. 1719 cm^{-1} is C=O stretch, 1450 cm^{-1} is C-H asymmetric deformation, 1151 cm^{-1} is C-O-C axial deformation, and 946 cm^{-1} is C-C stretch. The absence of an absorption band between 1500 and 1600 cm^{-1} shows that the previous removal of template molecules was effective.

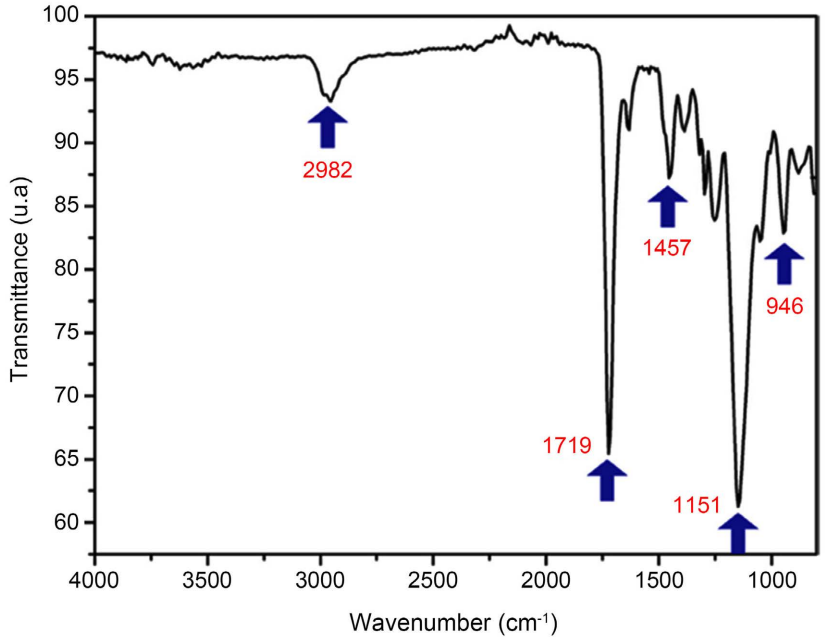

Figure 5. FTIR spectrum for the synthesized MIP with emphasis on the characteristic's bands.

3.3. UV Visible Spectrophotometry

The principle of UV visible spectrophotometry is based on the absorption characteristics of molecules under specific light conditions. Different compounds exhibit different absorbances at different wavelengths. By measuring the absorbance of sample solutions or gases, their chemical composition, concentration, and reaction kinetics can be determined.

The adsorption capacity of quinoxaline molecularly imprinted polymers was determined by using UV visible spectrophotometry. According to the standard curve method, a linear relationship between solution absorbance and solution concentration was plotted to calculate the mass concentration of the solution. The adsorption capacity of the polymer on the target substance was calculated using the formula [15].

Preparation of MIP: 0.32935 g Quinosislan, add 25 mL of chloroform, ultrasonic shaking and completely dissolve; add 421 μL of α-methacrylic acid, and after the shaking is sufficient, add 5.641 mL Ethylene glycol dimethacrylate with 5 min

shaking; rejoin 2.5% initiator Azodiisobutyronitrile, shaking for 5 - 10 min; the mixed solution was added dropwise to a 1% polyvinyl alcohol suspension at a rate of 2 drops/s using a drop funnel, heated in an oil bath at 75˚C, and condensed and refluxed; after a period of time, small purple solid particles were formed, and the reaction continued for 5 h, the temperature was raised to 90˚C, and the maturation was 2 h. Let it sit to allow the particles to settle and pour out the upper layer of liquid.

$$Q = (C_0 - C_1) \times m / V$$

In the formula: Q represents the adsorption capacity, μg/mg; C_0 represents OTA in the solution before adsorption Concentration, μg/mL; C_1 represents the concentration of OTA in the solution after adsorption, μg/mL; V is the volume of the solution, mL; M is the mass of the polymer, mg.

Chiral MIPs were prepared from the newly synthesized ATrp as functional monomers, and the effects of ATrp addition on the interaction with S-SUL, as well as the prepolymerization reaction of different molar ratios of S-SUL and ATrp in acetonitrile medium were studied by ultraviolet-visible light and fluorescence analysis [16].

Preparation of MIP: 0.0512 g S-SUL and 0.1548 g ATrp were added to 7.5 mL of acetonitrile and sonicated for 15 minutes to form a prepolymerized complex. Add 0.7128 g of EGDMA and 60.0 mg of AIBN and sonicate until well mixed. N_2 was injected and thermal polymerization was performed in a thermostatic water bath at 60˚C for 24 h. The resulting product was eluted with a methanol-acetic acid solution (v/v, 9:1) until S-SUL was undetectable on a 2550 UV-Vis spectrophotometer. After centrifugation, it is washed with methanol and sonicated into tiny particles. Finally, vacuum drying to constant weight to obtain a white powder.

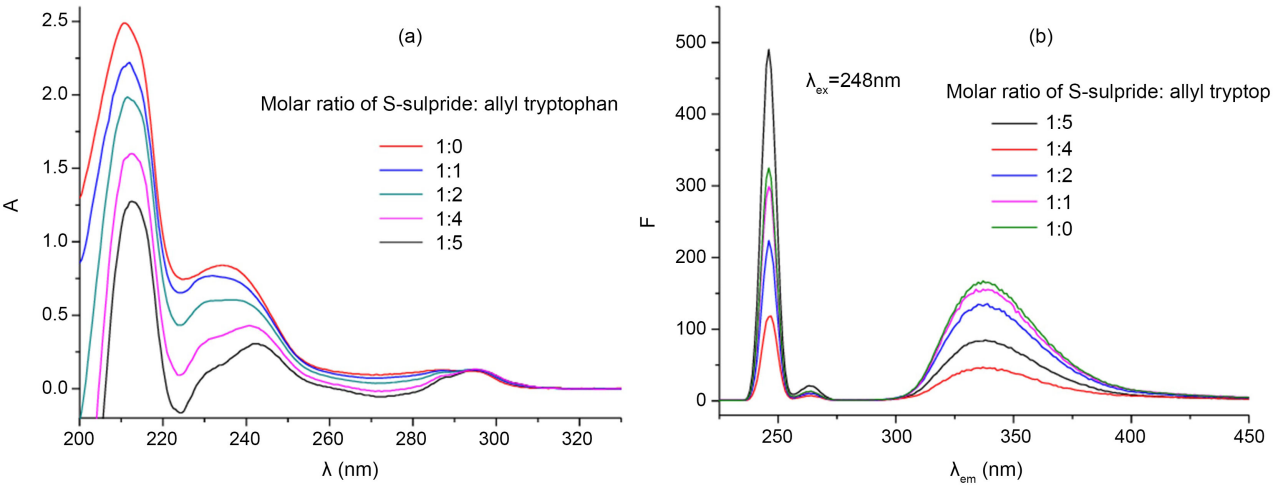

Figure 6. UV and fluorescence spectra for pre-polymerization reaction of S-sulpiride and N-acryloyl-tryptophan.

As can be seen from **Figure 6**, in **Figure 6(a)**, there are three adsorption peaks at 211, 234, and 286 nm. With the increase of ATrp dosage, the absorption intensity of each peak decreased, and the peak shifted to a longer wavelength, indicating

that S-SUL reacted with ATrp to form a stable complex. At the same time, the fluorescence emission spectra in Figure 6(b) can be further obtained, and the molar ratio of S-SUL to AT is 1:4, which is more suitable for the next preparation of MIP.

3.4. Transmission Electron Microscopy

The principle of transmission electron microscopy:

1) Absorption imaging: When electrons are emitted into a sample with high mass and density, the main phase formation is scattering. The areas with high mass and thickness on the sample have a larger scattering angle for electrons, fewer electrons pass through, and the brightness of the image is darker. Early transmission electron microscopes were based on this principle of TEM transmission electron microscopy.

2) Diffraction image: After the electron beam is diffracted by the sample, the amplitude distribution of the diffraction waves at different positions of the sample corresponds to the different diffraction abilities of each part of the crystal in the sample. When crystal defects appear, the diffraction ability of the defective part is different from that of the intact area, resulting in an uneven amplitude distribution of the diffraction bowl, reflecting the distribution of crystal defects.

3) Phase image: When the sample is thin to below 100 A, electrons can pass through the sample, and the amplitude change of the wave can be ignored. The imaging comes from the change in phase.

Transmission electron microscopy characterizes the surface morphology and agglomeration of magnetic samples to obtain high-resolution imaging of the samples. [17]

Preparation of magnetic chromium ion blotting polymer: 0.1 mmol potassium dichromate and 0.6 mmol salicylaldehyde oxime, a mixture of 50 mL of deionized water and isopropanol (volume ratio of 1:1), and magnetic stirring for 2 h at room temperature to obtain a Cr (VI.) complex. 0.1 g Fe_3O_4@mSiO_2 and 0.5 mmol α-methacrylic acid were weighed, added to 50 mL of isopropanol, ultrasonically dispersed for 15 min and then mixed with the complex, stirred for 1 h, 1.5 mL EGDMA and 50 mg AIBN were added, stirred, and the reaction vessel was sealed after N_2 for 15 min, and stirred at 60˚C for 24 h. At the end of the reaction, the product is separated by an external magnetic field and washed with ethanol and deionized water. Cr (VI.) in the blotting holes was extracted with shaking using 1 mol/L of NaOH solution as the eluent, and the amount of chromium ions in the wash solution was determined by atomic absorption spectroscopy until the solution no longer contained chromium ions, at which point the template was completely removed. The resulting product was dried at 60˚C for 12 h to obtain magnetic Cr (VI)-IIPs.

Figure 7 shows that core-shell structure of the magnetic carrier before polymerization is obvious, with a shell thickness of about 30 - 50 nm, and the shell surfaces are cross-linked with each other. The surface of b after the reaction is rough and

uneven, with improved dispersibility. This is mainly because the polymerization reaction mainly occurs in the shell layer with pores, resulting in the carrier surface being covered by a rough imprint layer, weakening magnetism. The imprint holes left after washing in the imprint layer can selectively adsorb Cr (VI).

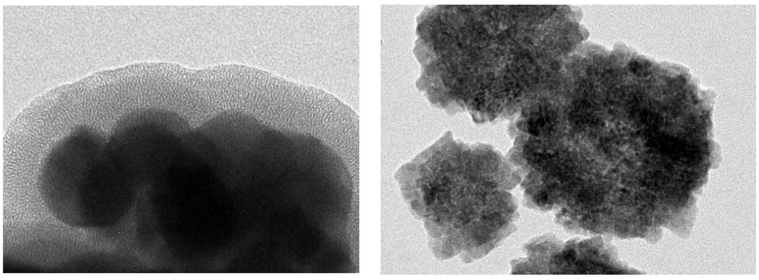

(a) (b)

Figure 7. Transmission electron microscopy of Fe_3O_4@mSiO_2 (a) and IIPs (b).

The surface morphology of MMIP and MNIP was characterized by SEM, and the morphological structure of MMIP was studied by TEM. By comparing particle sizes, it is possible to understand the reasons for the structural changes of polymers and the synthesis of polymers [18].

Preparation of MMIP: MMIPs prepared by 0.5 wt% MNP; 4-VP as a monomer and EDMA as a crosslinker in a ratio of 1:4:20.

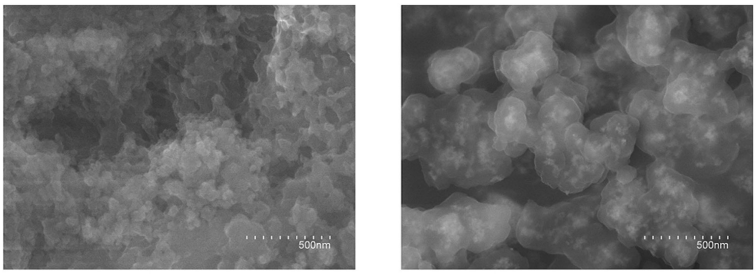

(a) (b)

Figure 8. SEM micrographs of the materials: (a) MMIPs and (b) MNIPs. Magnification scale at 30,000×.

As shown in **Figure 8**, the particle size of MMIP is lower than that of the control polymer (MNIP). This may be due to the fact that the template molecule has a certain influence on the growth of particles during the synthesis process, which affects the microstructure of the polymer. At the same time, it can be observed that the TEM image of the core containing the Fe_3O_4NPs agglomerate gives an average diameter of about 12 - 13 nm. The large size of the particle MMIPs (about 30 - 50 nm) indicates that MIPs were successfully synthesized by binding functional monomers and crosslinkers on the magnetite surface. The texture properties of the material were also investigated by nitrogen adsorption-desorption measurements. The results showed that the specific surface area of MMIPs was higher than that of MNIPs. The MMIP gives an aperture larger than the corresponding MNIP. Then, it was concluded that the formation of selective cavities

was successfully produced in MMIP.

3.5. Thermogravimetric Analysis

The principle of thermogravimetric analysis: In order to keep the sample under a certain temperature program (rise/fall/constant temperature) control, observe the process of the quality of the sample changing with temperature or time. It can measure the thermal stability and oxidation stability of materials under different atmospheres, analyze the physicochemical processes such as decomposition, adsorption, desorption, oxidation, and reduction, quantitatively calculate the composition of substances, and determine the content of moisture, volatile components, and various additives and fillers.

By using thermogravimetric analysis to analyze the thermal stability and mass loss rate of polymers, it is concluded that imprinted polymers have better rigidity and are insensitive to environmental temperature, making them suitable for general usage conditions [17].

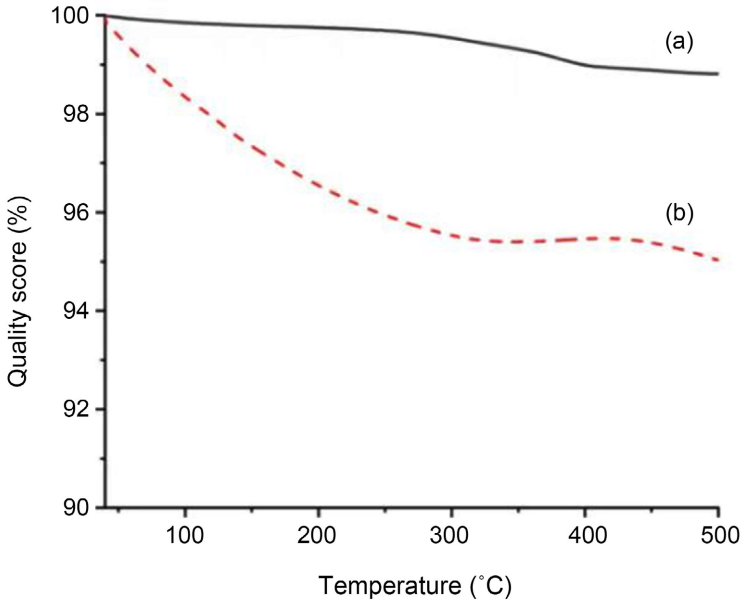

Figure 9. Thermogravimetric analysis of IIPs (a) and NIPs (b).

By plotting the thermogravimetric analysis of both, as shown in the figure (**Figure 9**), after the polymerization reaction, both a and b exhibit good thermal stability. When the temperature reaches 500˚C, the mass loss of a is only about 1%, while the mass loss of b is about 6%. However, b shows a faster mass loss rate compared to a. This is because the imprinted holes formed by a during preparation are more ordered than b due to the presence of target ions, resulting in better rigidity of the imprinted polymer and insensitivity to environmental temperature, making it suitable for general usage conditions.

Thermogravimetric analysis is performed in the presence of nitrogen using a thermogravimetric analyzer. The analysis of the mass loss curve and the derivative

curve of mass loss provides an idea of the stability of the polymer at high temperatures, as well as the temperature at which the thermal degradation reaction occurs and the maximum degradation rate [19].

Preparation of MIP:

1) Emulsion polymerization: 1.55 g of polyvinyl alcohol and 0.1078 g of dodecyl sulfate dissolved in 75 mL of hot water in a fat-bottom flask, stirred with a magnetic stir bar under nitrogen at a speed of 250 rpm and sealed. A pre-polymerization mixture was prepared in a separate flask by dissolving the template molecules (diclofenac 60 mg, sodium and naproxen 50 mg) and functional monomers (methacrylic acid 85 μL or 2-vinylpyridine 110 μL) in 2 mL of methanol and 4 mL of the pore-forming agent toluene. The mixture was supplemented with 2 mL of the crosslinker ethylene glycol dimethacrylate and 150 μL of the initiator azodiisobutyronitrile and stirred with a magnetic stir bar at 250 rpm until completely dissolved. Add the prepolymerized mixture drop by drop through a syringe; Maintain at 70˚C in a glycerol bath with continuous agitation at 100 rpm for 24 h. Finally, the polymer is obtained and washed with hot water.

2) Bulk polymerization: template (diclofenac 60 mg, sodium and naproxen 50 mg) and monomer (methacrylic acid 85 μL or 2-vinylpyridine 110 μL) were mixed at 250 rpm under magnetic stirring, and methanol 2 mL, crosslinker ethylene glycol dimethacrylate 2 mL, initiator azodiisobutyronitrile 150 μL, and pore-forming agent toluene, 4 mL; 2 mL of the crosslinker ethylene glycol dimethacrylate 150 μL of the initiator azodiisobutyronitrile and 4 mL of the pore-forming agent toluene were added. Perform under nitrogen without agitation in a glycerol bath at 70˚C for 24 h.

3) Co-precipitation polymerization: Same procedure and reaction conditions as the bulk polymerization, but with the addition of toluene 20 mL and solvent methanol 10 mL, stirred at 70˚C for 24 hours at 100 rpm constant magnetism.

Figure 10 shows the quality loss curve for each evaluation. As can be seen from the diagram, all polymers lose water at the initial step, up to about 100˚C. MB-NPX-04 polymer has the lowest stability, with a weight loss of 75% at 400˚C. MB-IBP-04 is the most stable MIP, with a weight loss rate of 60% at 400˚C. For all three MIPs, thermal stability of around 300˚C was observed, confirming that these materials can withstand critical operating conditions.

Figure 11 shows the derivative of the mass loss curve. As can be seen from the figure, the thermal degradation of polymer materials occurs in one or two steps. ME DCF-01 mainly starts at around 200˚C, has a maximum degradation rate at 363˚C, and has a weight loss of 35%, stopping at around 460˚C. MB-NPX-03 polymer has a maximum degradation rate at 345˚C with a weight loss of 42%, and a single thermal degradation step starts at around 250˚C and ends at around 440˚C. Thermal degradation of MB-IBP-04 is carried out in two steps. The main step starts at around 250˚C, with a maximum degradation rate at 319˚C and a weight loss of 32%, ending at around 440˚C. The maximum degradation rate in the second step is about 400˚C.

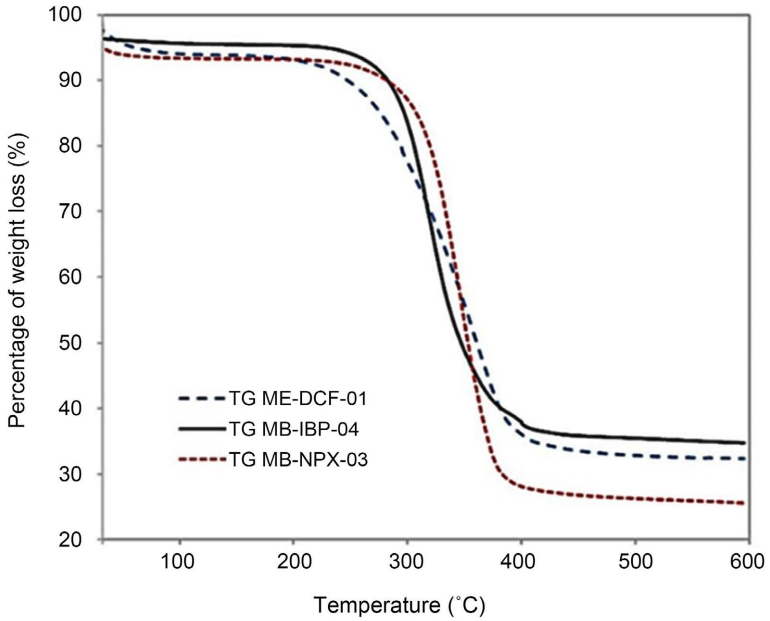

Figure 10. TGA curves for the imprinted polymers: ME-DCF-01, MB NPX-03, and MB-IBP-04.

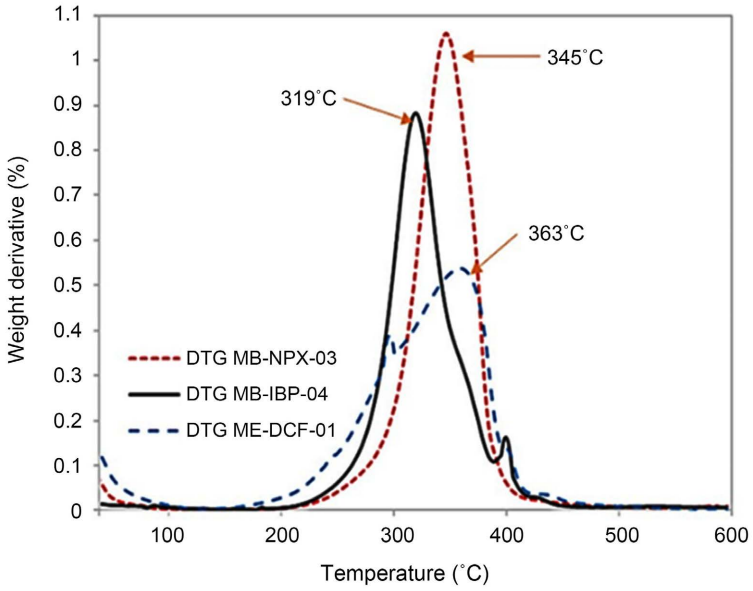

Figure 11. dML analysis for the imprinted polymers: ME-DCF-01, MB NPX-03, and MB-IBP-04.

3.6. Laser Particle Size Analyzer

Working principle of laser particle size analyzer: By utilizing the absorption, scattering, and transparency characteristics of laser in the sample, when the laser irradiates particles in the sample, scattering phenomenon occurs, that is, a part of the laser will reflect, deflect, and refract on the surface of the particles, forming different scattering angles and intensities. Obtain relevant physical parameters such as particle size and distribution patterns through detection, calculation, and

analysis.

Using Mastersizer 2000 laser particle size analyzer to analyze the particle size of synthesized spherical products, plot their particle size distribution, obtain parameters such as particle size distribution range, volume average particle size, and corresponding particle size for capping, which can better determine the particle size range for filling the solid-phase extraction column. On the premise of ensuring that the polymer particles are small enough, it is not only necessary to consider that most polymer particles will not seep out of the sieve plate, but also to ensure that the polymer particle size has a gradient change to better fill the space in the solid-phase extraction column, thereby improving the unit adsorption efficiency [13].

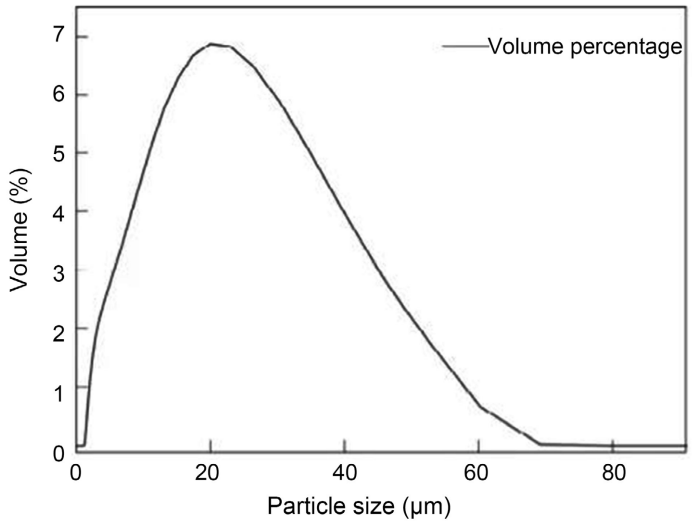

Figure 12. Particle size distribution of spherical toluene molecularly imprinted polymers.

As shown in **Figure 12**, we can see that the particle size distribution range is 1 - 70 μm. The average volume particle size is 16.795 μm. Peak corresponds to a particle size of 20.3 μM. In theory, the smaller the particle size of polymer microspheres, the higher the imprinting efficiency per unit mass of the imprinted polymer. Therefore, the particle size of polymer should be controlled to be small enough to improve their adsorption efficiency. The design purpose of toluene molecularly imprinted polymer is to serve as an extraction filler for toluene molecules in solid-phase extraction devices, and the pore size of the sieve plate at the bottom of the standard solid-phase extraction column is 20.0 μm. This means that the batch of molecularly imprinted polymers with a small particle size less than 20.0 were screened out μM microspheres can be directly used for solid-phase extraction of toluene molecules.

Laser diffraction and scanning electron microscopy were used to characterize the particle size distribution and surface structure morphology of MIP, respectively, and NIP was used as a reference to further analyze the difference of mesostructure from macroscopic and microscopic perspectives [16].

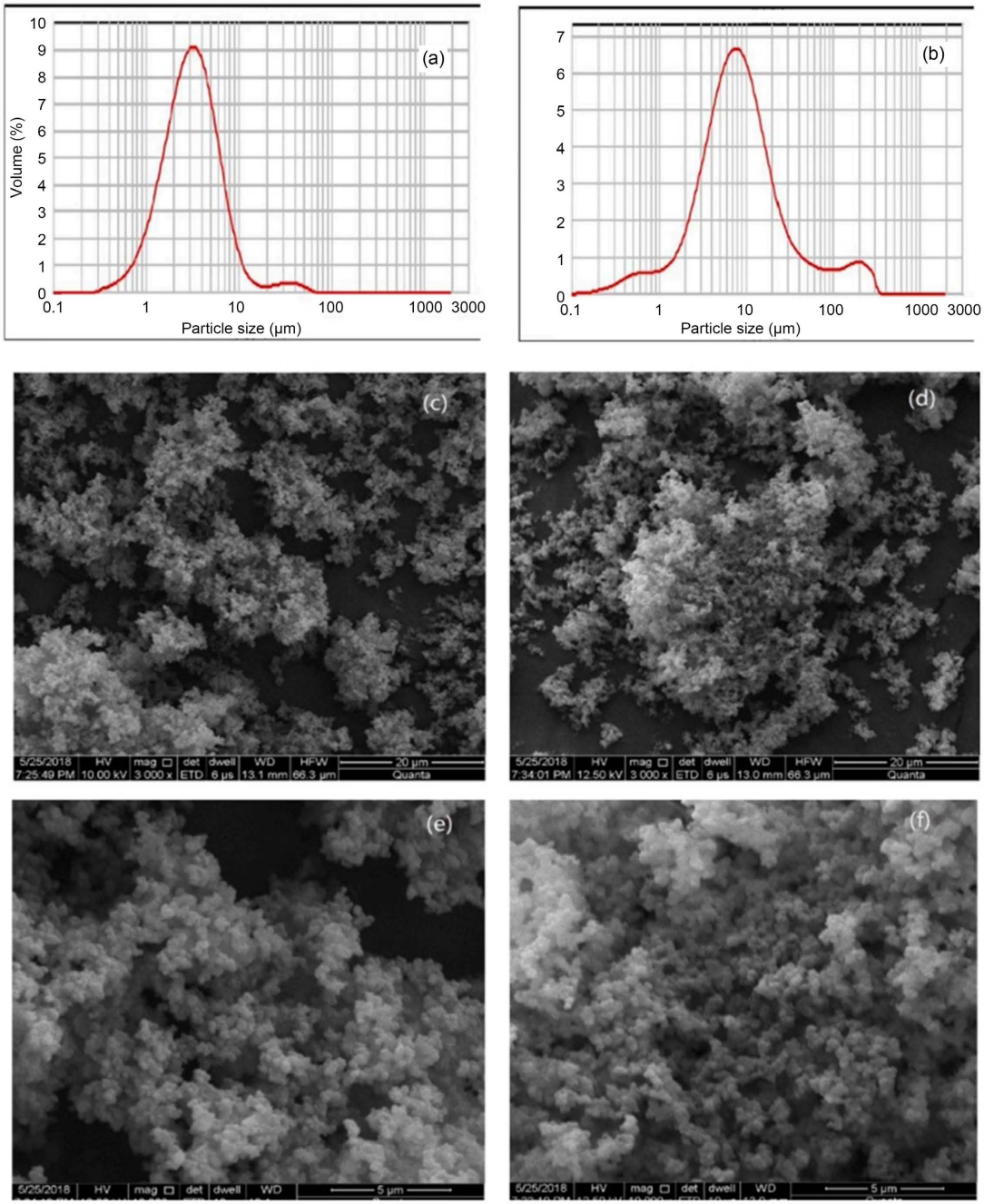

Figure 13. Particle size distribution and scanning electron microscopy (SEM) images of the materials: the MIP (a, c and e) and the NIP (b, d and f).

From a macroscopic perspective, MIP and NIP prepared by bulk polymerization are homogeneous white microsphere particles. Their morphological images at the microscopic level differ from each other. By looking at Figure 13, we can find out: the particle size of MIP is smaller and more uniform than that of NIP. Based on the SEM images, the mesoscopic structural differences between MIP and NIP are very significant. At the microscopic level, (c)-(f) show that both polymers exhibit a tufted pore structure, but NIP has a tighter tufted structure. In comparison,

the surface structure of MIP is looser and more porous than that of NIP. As a result, the resulting polymer is easily dispersed into unformed particles by ultrasonication, thus avoiding damage to the surface structure caused by grinding, while these hard and lumpy MIPs need to be ground and sieved before use. To a certain extent, mechanical processes will inevitably destroy the surface structure and imprint cavities.

4. Conclusion

In this paper, the molecular imprinting technique is described from the background, theory and characterization methods, and the following is a summary of each characterization method:

name	Test Method	Function
Langmuir equation	Based on experimental data, the Langmuir adsorption isothermal formula was fitted.	1) The maximum adsorption capacity can be obtained by bringing in the equation calculation, and the saturation adsorption capacity can be compared with the saturation adsorption capacity to determine whether the adsorption reaches saturation. 2) Compare the adsorption capacity and analyze the difference in adsorption behavior.
Infrared spectroscopy	The characteristic beam derived from the infrared spectrometer is used for peak beam analysis.	1) Determine the possible presence of functional groups in the polymer, and then infer the structure of the polymer. 2) Analyze the functional groups, compare them with the template molecules, and obtain the removal of template molecules.
UV-Vis spectrophotometry	The absorbance of a sample solution or gas is measured using the absorption of a UV-Vis spectrophotometer at a specific light.	1) According to the standard curve method, the standard curve is drawn with the linear relationship between the absorbance of the solution and the concentration of the solution, the mass concentration of the solution is calculated, and the adsorption amount of the polymer to the target is calculated according to the formula. 2) Measure the influence of different amounts of reagents on polymer interaction, and obtain the optimal molar ratio through the trend of absorption intensity and wavelength of the absorption peak.
Transmission electron microscopy	The surface morphology of the polymer was characterized by transmission electron microscopy and the imaging image of the sample was obtained.	1) The characterization of magnetic samples can further analyze the morphology of polymerized and unpolymerized carriers, as well as the causes of polymerization. 2) Through the comparison of particle size, we can understand the reasons for the structural change of polymers and the synthesis situation.

Continued

Thermogravimetric analysis	The sample is subjected to a certain temperature program (rise/fall/constant temperature) control, and the quality of the sample is observed with temperature or time.	1) The thermal stability and mass loss rate of the polymer can be analyzed. 2) By analyzing the mass loss curve and the derivative curve of mass loss, we can know the stability of the polymer at high temperature, as well as the temperature and maximum degradation rate of the thermal degradation reaction.
Laser particle size analyzer	Using the absorption, scattering and transparency of the laser in the sample, the particle size and its distribution law and other related physical parameters were analyzed.	1) The particle size of the polymer is analyzed, and its particle size distribution is graphed to obtain its particle size distribution range, volume average particle size, capping corresponding particle size and other parameters, so as to determine the particle size range of the solid phase extraction column, so as to improve the unit adsorption efficiency. 2) The particle size distribution and surface structure morphology of MIP were characterized, and NIP is used as a reference. Further analysis of the mesoscopic structural differences revealed that the resulting polymers are easily dispersed into unformed particles by ultrasonication, thus avoiding surface structure damage caused by grinding.

In the characterization of polymers, not only one of the methods is used, but a variety of methods are used to analyze the polymers, to make the research more scientific and rigorous. At the same time, the above methods are not all the methods for the characterization of imprinted molecular polymers in modern science, but only a list of some methods that are commonly used by people and can also be used well for experimental analysis. With the development of MIPs and characterization methods, more methods are expected to emerge in the future to help characterize the features and performances of MIPs.

Conflicts of Interest

The author declares no conflicts of interest regarding the publication of this paper.

References

[1] Shi, X., Wang, Q. and Zhang, Y. (2024) Application Progress of Surface Molecular Imprinting Technology in Food Sample Pretreatment. *Food Science*, **45**, 282-294.

[2] Hou, M., Sun, D., Yan, L., Fu, L., Wang, H., Yu, J. and Liu, H. (2024) Research Progress on Molecular Imprinting Solid-Phase Extraction for the Determination of Antibiotic Residues in the Environment and Food. *Analytical Laboratory*.

[3] Xie, C., You, Z., Feng, J., Zhang, X. and Wu, X. (2023) Research Progress in the

Preparation and Environmental Applications of Antibiotic Molecularly Imprinted Polymers. *Journal of Zhaoqing University*, **44**, 1-8.

[4] Sun, M., Du, X., Chen, G., Zhang, H., Chen, J., Li, H. and He, J. (2023) Preparation and Application of Molecularly Imprinted Polymers on the Surface of Renzaiwei for Sample Pretreatment. *Analysis Laboratory*, **43**, 1259-1265. https://doi.org/10.13595/j.cnki.issn1000-0720.2023060204

[5] Wang, Y., Liu, C., Yang, Z., Duan, E., Zhao, Y., Qiao, H. and Wang, J. (2024) Application of Molecular Imprinting Technology in the Detection of Macrolide Drugs. *Feed Research*, **47**, 172-176.

[6] Jia, M., Meng, X., Zhao, L., Huang, Y. and Liu, Z. (2024) Microfluidic Synthesis and Performance Study of Mangiferin Imprinted Polymers. *Guangdong Chemical Industry*, **51**, 14-17.

[7] Jiang, F. (2023) Preparation of Biocompatible Photoresponsive Surface Molecularly Imprinted Polymers and Study on the Delivery of Anticancer Drug Molecules. Master's Thesis, Southwest University.

[8] Jiang, Z., Guo, W., Li, Z., Hou, H., Huo, W., Wang, J., Ma, L., Jin, H., Huang, Y. and Zhang, R. (2024) Preparation of Macroporous Anion Exchange Chromatographic Medium by Grafting Polyamine Polymer and Evaluation of Its Protein Adsorption Behavior. *Chinese Journal of Chromatography*, **42**, 360-367.

[9] Sun, X. (2018) Preparation and Application of Poly (MAA co EDMA) Polymer Microspheres and Benzophenone Based Molecularly Imprinted Polymers. Master's Thesis, Huazhong University of Science and Technology.

[10] Chu, G., Wu, K. and Xiao, W. (2018) Synthesis of Resveratrol Molecularly Imprinted Polymers Polymerized by Active Free Radicals and Their Application in the Analysis of Resveratrol in Grape Peels. *Journal of Functional Materials*, **49**, 11127-11131.

[11] Dou, P. (2019) Preparation and Characterization of Lutetium (III) Ion Imprinted Polymers. *Rubber and Plastics Technology and Equipment*, **45**, 1-5.

[12] Abu-Alsoud, G.F., Hawboldt, K.A. and Bottaro, C.S. (2020) Comparison of Four Adsorption Isotherm Models for Characterizing Molecular Recognition of Individual Phenolic Compounds in Porous Tailor-Made Molecularly Imprinted Polymer Films. *ACS Applied Materials & Interfaces*, **12**, 11998-12009. https://doi.org/10.1021/acsami.9b21493

[13] Ma, Y., Zheng, H., Liu, Y., *et al.* (2018) Synthesis and Characterization of Toluene Molecularly Imprinted Polymers Based on Precipitation Polymerization. *Contemporary Chemical Industry*, **47**, 2002-2005.

[14] Silva, C.F., Menezes, L.F., Pereira, A.C. and Nascimento, C.S. (2021) Molecularly Imprinted Polymer (MIP) for Thiamethoxam: A Theoretical and Experimental Study. *Journal of Molecular Structure*, **1231**, Article 129980. https://doi.org/10.1016/j.molstruc.2021.129980

[15] Xu, P., Wu, C., Song, L., *et al.* (2021) Synthesis and Characterization of Quinone Blue Molecularly Imprinted Polymers. *Modern Chemical Industry*, **41**, 208-211.

[16] Wang, L., She, X., Chen, Z., Quan, S., Liu, Y., Mai, X., *et al.* (2021) Preparation and Characterization of a Chiral Molecularly Imprinted Polymer with a Novel Functional Monomer for Controlled Release of S-Sulpiride. *International Journal of Pharmaceutics*, **601**, Article 120526. https://doi.org/10.1016/j.ijpharm.2021.120526

[17] Guo, C. (2021) Preparation and Performance Characterization of Chromium Ion and 4,4'-Diaminodiphenylmethane Imprinted Polymers. Master's Thesis, Jiangnan University.

[18] Meseguer-Lloret, S., Torres-Cartas, S., Gómez-Benito, C. and Herrero-Martínez, J.M.

(2022) Magnetic Molecularly Imprinted Polymer for the Simultaneous Selective Extraction of Phenoxy Acid Herbicides from Environmental Water Samples. *Talanta*, **239**, Article 123082. https://doi.org/10.1016/j.talanta.2021.123082

[19] Meléndez-Marmolejo, J., Díaz de León-Martínez, L., Galván-Romero, V., Villarreal-Lucio, S., Ocampo-Pérez, R., Medellín-Castillo, N.A., *et al.* (2022) Design and Application of Molecularly Imprinted Polymers for Adsorption and Environmental Assessment of Anti-Inflammatory Drugs in Wastewater Samples. *Environmental Science and Pollution Research*, **29**, 45885-45902. https://doi.org/10.1007/s11356-022-19130-0